THE ASTROPHYSICAL JOURNAL, 465:534–547, 1996 July 10

BRIGHTEST CLUSTER GALAXY PROFILE SHAPES

ALISTER GRAHAM,[1] TOD R. LAUER,[2,3] MATTHEW COLLESS,[1] AND MARC POSTMAN[4,5]
Received 1995 December 18; accepted 1996 February 2

ABSTRACT

We model the surface brightness profiles of a sample of 119 Abell brightest cluster galaxies (BCGs), finding a generalized de Vaucouleurs $R^{1/n}$ law, where n is a free parameter, to be appropriate. Departures from the $R^{1/4}$ law are shown to be a real feature of galaxy profiles and not due to observational errors or coupling of n with the other model parameters. BCGs typically have values of n greater than 4. The shape parameter n is shown to correlate with effective half-light radius, such that the larger BCGs have larger values of n. This continues a trend noticed amongst ordinary elliptical galaxies and dwarf elliptical galaxies, such that the brighter galaxies have larger values of n.

Subject headings: galaxies: clusters: general — galaxies: elliptical and lenticular, cD — galaxies: photometry — galaxies: structure

1. INTRODUCTION

The structure of the first-ranked members of Abell clusters, or brightest cluster galaxies (BCGs), has long been of interest given that these galaxies can be used as standard candles for exploring the large-scale structure of the universe (Humason, Mayall, & Sandage 1956; Sandage 1972a, b; Gunn & Oke 1975; Lauer & Postman 1994). Hoessel (1980), for example, developed the L-α relationship, which relates BCG structure to their luminosities through fixed physical apertures, thus reducing the cosmic scatter in the aperture luminosities. Understanding the L-α relationship has been of particular interest recently, given its use by Lauer & Postman (1992, 1994) to probe the linearity of the Hubble flow and to detect large-scale bulk flows out to the 15,000 km s^{-1} scale. The structure of BCGs may also reflect galactic cannibalism (Ostriker & Tremaine 1975; Hausman & Ostriker 1978; Hoessel 1980; Schneider, Gunn, & Hoessel 1983), where other cluster members may be captured through dynamical friction, changing both the luminosity and the shape of the dominant BCG.

While to first order BCGs appear to be ordinary, if highly luminous, elliptical galaxies, in many ways they are a special class of objects. Tremaine & Richstone (1977) showed, for example, that their luminosity function was not consistent with them being drawn simply as the brightest member of a standard Schechter (1976) luminosity function. Oemler (1976) showed that as a class, BCGs differed structurally from other giant elliptical galaxies of similar luminosity, having more extended limiting radii at a given total luminosity than other giant elliptical galaxies. Schombert (1986) conducted an extensive survey of BCG brightness profiles, finding them to be shallower than those for more ordinary elliptical galaxies, such that the BCGs were always more extended at a given surface brightness level than would be suggested by simply scaling by total luminosity. Hoessel, Oegerle, & Schneider (1987) also concurred with this, showing BCGs to follow a shallower (and tighter) relationship between effective radii, r_e, and effective surface brightness, I_e, than do ordinary elliptical galaxies (Oegerle & Hoessel 1991; Graham 1996). This distinction in form was additionally interesting as Schombert (1986) showed it to arise in the relatively brighter midportions of the BCG profile, regardless of whether or not the BCG had additional envelopes at faint surface brightness making them cD galaxies as well. A cD galaxy is a giant elliptical that has a separate extended low surface brightness envelope, which is evident as an inflection in the brightness profile (Oemler 1976)—typically at $\mu_V \sim 24$ or greater (Kormendy & Djorgovski 1989).

Schombert (1986) emphasized that the classic $R^{1/4}$ law, introduced by de Vaucouleurs (1948, 1953) to describe elliptical galaxies at all luminosities, was often a poor match to the BCG profiles, in many cases fitting the profiles only over a restricted range of surface brightness. Looking at the profiles presented by Schombert (1986), it becomes apparent that many of the BCGs would be better fitted by power laws rather than $R^{1/4}$ laws. This is also found to be the case in Ledlow & Owen's (1995) work with galaxies in rich clusters. This appears to have little to do with whether or not a BCG is also a cD galaxy. An additional caveat is that because a constant power law will rise above an $R^{1/4}$ law at large radii, a cD envelope may be erroneously detected as a separate component in $R^{1/4}$ plots, even though a single power law could describe the BCG completely. In short, classification of a BCG as cD or not is problematic; our present investigation, however, is not affected by this issue, since this apparently has little to do in any case with the distinct overall structural properties of BCGs compared to those of giant elliptical galaxies.

If some BCGs are better described by power laws, and others by $R^{1/4}$ laws, an inspection of the profiles presented by Schombert (1986) shows that BCGs fall along a contin-

[1] Mount Stromlo and Siding Spring Observatories, Australian National University, Private Bag, Weston Creek PO, ACT 2611, Australia.
[2] Kitt Peak National Observatory (KPNO), National Optical Astronomy Observatories (NOAO), P.O. Box 26732, Tucson, AZ 85726. NOAO is operated by the Association of Universities for Research in Astronomy (AURA), Inc., under cooperative agreement with the National Science Foundation.
[3] Visiting Astronomer, Cerro Tololo Inter-American Observatory (CTIO), NOAO.
[4] Space Telescope Science Institute,[6] 3700 San Martin Drive, Baltimore, MD 21218.
[5] Visiting Astronomer, KPNO and CTIO.
[6] Space Telescope Science Institute is operated by AURA, Inc., under contract to the National Aeronautics and Space Administration.

uum between the two forms. We are thus motivated to advance the Sersic (1968) form, which includes both laws as a better description and generalization of BCG brightness profiles. In the Sersic form, $I(r) \propto \exp[-(r/r_e)^{1/n}]$, where n is a free parameter. For $n = 1$ this is an exponential disk; for $n = 4$ it is a de Vaucouleurs profile; and as $n \to \infty$ it asymptotes to a power law of index -2.

Young & Currie (1994) fitted the Sersic form to a sample of dwarf elliptical (dE) galaxies, showing a correlation between galaxy absolute magnitude and the shape parameter n, such that the fainter galaxies had the smaller values of n. The same pattern in profile shape had also been noted by Davies et al. (1988). Working with a sample of Fornax low surface brightness (LSB) diffuse dwarf elliptical and spheroidal galaxies, they showed a trend between n and the logarithm of the scale radius r_e, such that the scale radius increased as n increased. Caon, Capaccioli, & D'Onofrio (1993) showed that this trend extended into the domain of ordinary elliptical galaxies. It has also recently been shown to hold for the bulges of spiral galaxies by Andredakis, Peletier, & Balcells (1995) and Courteau, de Jong, & Broeils (1996).

We are now in an excellent position to explore the systematics of the BCG structural properties as Postman & Lauer (1995) present a complete and volume-limited sample of BCGs out to 15,000 km s^{-1}. The data were obtained with large-area CCDs and reduced with photometric uniformity in mind, given the goal to use this data set to detect the subtle effect of bulk flows on the $L - \alpha$ relationship residuals (Lauer & Postman 1994). Here we show that the correlation between n and scale radius (Caon et al. 1993) extends to BCGs, where n is typically greater than 4, whereas for the dE it is seen to be less than 4. The existence of this relation across such a large range of galaxy sizes must be telling us something fundamental about the structure and formation processes of elliptical galaxies in general.

In the next section we present some of the theory behind the $R^{1/n}$ model. Section 3 presents the BCG surface brightness data and the parameterized model fits to it. In § 4 we discuss the results of the model fitting and compare this in the context of work on other galaxies in § 5. We investigate how n relates to other measures of galaxy structure, both local (§ 6) and global (§ 7). Our conclusions are given in § 8.

2. THE $R^{1/n}$ LAW

The $R^{1/n}$ law gives the observed galaxy intensity, I, as a function of radius such that

$$I(r) = I_e \exp\left\{-b\left[\left(\frac{r}{r_e}\right)^{1/n} - 1\right]\right\}, \quad (1)$$

where I_e is the intensity at the radius r_e. The constant b is chosen so that r_e becomes the radius enclosing half of the total light from the galaxy. This generalized de Vaucouleurs law was introduced by Sersic (1968) and further developed by Ciotti (1991); the de Vaucouleurs law has $n = 4$ and $b = 7.67$. Note that the constant b in this formula is a function of n. The generalized expression can be written as

$$\mu(r) = \mu_0 + \frac{2.5 b_n}{\ln(10)}\left(\frac{r}{r_e}\right)^{1/n}, \quad (2)$$

with r_e the scale radius, μ_0 the central surface brightness, and b_n the function of n given below. Again we select b_n so that r_e is the radius enclosing half of the total light for the $R^{1/n}$ model. For $n = 4$ the well-known de Vaucouleurs $R^{1/4}$ formula, $\mu = \mu_0 + 8.33(r/r_e)^{1/4}$, is recovered. The luminosity interior to the radius r is given by

$$L(r) = I_e r_e^2 \, 2\pi n \frac{e^{b_n}}{(b_n)^{2n}} \gamma(2n, x), \quad (3)$$

where $\gamma(2n, x)$ is the incomplete gamma function with $x = b_n(r/r_e)^{1/n}$, defined by

$$\gamma(2n, x) = \int_0^x e^{-t} t^{2n-1} \, dt. \quad (4)$$

Thus, the value of b_n is such that $\Gamma(2n) = 2\gamma(2n, b_n)$, where Γ is the gamma function. As given by Capaccioli (1989), this can be well approximated by $b_n \approx 2n - 0.327$.

The differences between an $R^{1/n}$ model and an $R^{1/4}$ model are best described graphically. In Figure 1, we plot these differences for n ranging from 1 to 10. Following Capaccioli (1989), the models have been constructed to have the same total luminosity in units of I_e. The abscissa is in units of the half-light radius of the $R^{1/4}$ model. As n climbs greater than 4, the curvature in the profile is steadily removed until it asymptotes to $\mu(r) = \mu_e + 5 \log r$. As n exceeds 10, the

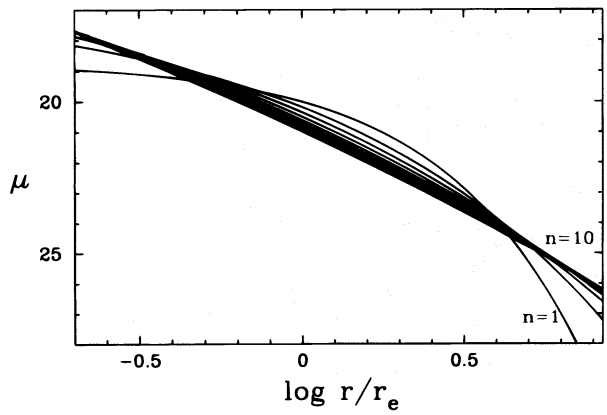

FIG. 1a

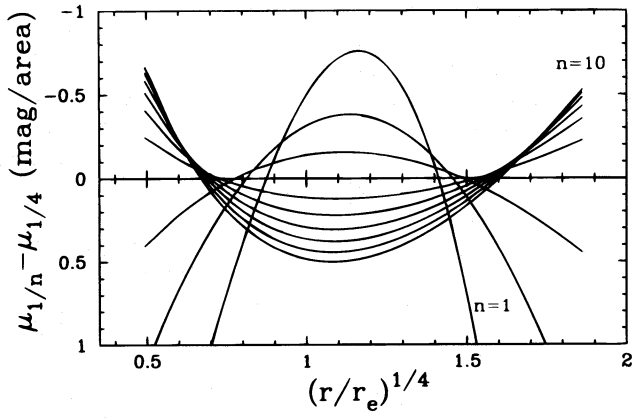

FIG. 1b

FIG. 1.—(*a*) Surface brightness profiles of an $R^{1/n}$ law, for integer values of n ranging from 1 to 10. (*b*) Difference between the surface brightness profiles of an $R^{1/n}$ and an $R^{1/4}$ law, for n ranging from 1 to 10 in steps of 1. All profiles give the same total magnitude, in units of I_e^n.

differences in the profiles become less marked. As $n \to \infty$ the $R^{1/n}$ profile asymptotes to $I \propto (r/r_e)^{-2}$. It is seen that for the range in radius that can be matched by observations, values of $n < 4$ lead to a hump in the profile indicating that the $R^{1/4}$ profile is too faint for the central parts and too bright to match the inner and outer portions of the profile. The situation is reversed for $n > 4$, such that the brighter galaxies have more light at larger radii than the $R^{1/4}$ law allows.

3. OBSERVATIONAL SURFACE BRIGHTNESS PROFILES AND FITTED MODELS

The galaxies studied here are the BCGs of the volume-limited sample of the 119 Abell clusters known to be within 15,000 km s^{-1}, which were selected by Lauer & Postman (1994) to define a large-scale inertial reference frame. Full details of the galaxy selection, observations, and data reduction are given in Postman & Lauer (1995), but we summarize them briefly here. BCG candidates were selected from sky survey images and imaged in the Kron-Cousins R band under photometric conditions with large-area CCD cameras at KPNO and CTIO. The distance indicator used by Lauer & Postman (1994) is based on the integrated luminosity of the BCG within the central 10 h^{-1} kpc metric aperture; thus, final selection of a given galaxy as "brightest" among rival candidates is by metric rather than total luminosity. On this note, Postman & Lauer (1995) emphasize that a number of their BCG identifications differ from those made earlier by Hoessel (1980).

Postman & Lauer (1995) measured profiles of the BCGs using the multi-isophote fitting algorithm of Lauer (1986). Many of the BCGs are part of multiple-galaxy systems; the multi-isophote algorithm solves for the brightness distributions of all overlapping galaxies simultaneously. Compact galaxies, stars, CCD defects, and so on, can also be excluded from the isophote fitting algorithm. Final accuracy of the profiles is limited by photometric calibration at small radii, and sky-subtraction errors at large radii. Postman & Lauer (1995) used repeat observations of the same galaxies to show that the basic random error in the BCG aperture magnitudes is only 0.014 mag; the surface brightness values for isophotes within the metric radius will be accurate to a similar level. Errors in the photometry due to sky-subtraction errors will begin to dominate outside the metric radius but should still be at the few percent level at the limiting isophote brightness adopted here of $\mu_R = 23.5$. Postman & Lauer (1995) did sky subtraction using a mode estimator in the image corners. Some BCGs were still contributing significant amounts of light at the edges of even the large fields of the CCDs used, in which cases additional observations were obtained offset from the primary galaxy image to measure the sky at larger angular distances from the BCGs. Finally, we note that the galaxy profiles are presented as observed. No K or extinction corrections have been applied (although Postman & Lauer (1995) did apply them to derive BCG metric absolute luminosities).

The model profiles have been fitted to the data outside of the central 3″, because of the possible influence of core structure that is separate to the outer galaxy profile. We also have not used the profile data fainter than 23.5 mag to be sure we are not affected by sky-subtraction errors. In addition, this level of truncation in the profile ensures that our results are not a product of the extended halos or envelopes that cD galaxies are known to have. For many of the BCGs we had multiple images and could directly compare different profiles of the same galaxy for agreement. The model parameters obtained for galaxies with multiple images are found to be in agreement with each other within the errors.

Equation (2) has been fitted to the semimajor axis surface brightness profiles of the BCGs, using a simple error weighting scheme based on the S/N of each data point, via standard nonlinear least-squares to solve for the three unknowns. We give here the superscript n to the value of μ_0 and r_e derived from the $R^{1/n}$ formula, to prevent confusion with the values derived from the $R^{1/4}$ formula. $\Delta\chi^2$ ellipsoids were computed around the best-fitting parameters, μ_0^n, r_e^n, and n. This was done by moving through a fine three-dimensional grid of values and computing the value of χ^2 at each point. r_e was converted to log r_e and the ellipsoids then projected onto the relevant two-dimensional plane.

In addition, we fitted for the standard $R^{1/4}$ formula, where the value of n is fixed at 4 and one solves for μ_0 and r_e. We also explored the use of a power law to describe the light profiles. The method of least squares was used to fit the profiles to

$$\mu(r'') = A + B \log (r'') , \tag{5}$$

where A is referred to as the intercept and is approximately the central surface brightness, being the value at $r = 1''$. B is the slope of this power law. We divide B by -2.5 so that it reflects the slope of the log (intensity) $-$ log (radius) profile. Future references will refer to this modified value of B as being the slope. For the very flattened profiles, $n > 15$, the profiles lacked any significant curvature and it was appropriate to fit a power law of the above form to the data. The $R^{1/n}$ law is also restrictive when dealing with large n as it tends to a power law of fixed slope, being -2.

4. BRIGHTEST CLUSTER GALAXY PROFILES

The various profiles, $R^{1/4}$, $R^{1/n}$, and a simple power law, have been fitted to the BCG surface brightness profiles and are displayed in the Appendix. The residuals of the data about these best-fitting models is shown clearly in Figure 2 for a handful of galaxies, as are the measurement uncertainties, based on S/N measurements, associated with the data. In general, one finds that the $R^{1/4}$ law has too much curvature to match the data, resulting in a negative bowl-shaped residual profile. The opposite is found for the fitting of a power law, where one generally finds the profile data have some level of curvature that cannot be accounted for with a simple power law, resulting in a positive hump in the residual profile. The $R^{1/n}$ model with its free shape parameter can account for the differing levels of curvature and thus provides the best fit to the data, ironing out the large-scale departures seen in the above two models. The BCG profiles show a continuum of behavior, ranging smoothly from profiles that are $r^{1/4}$-like to those that are power laws. We find that the Sersic form covers this issue nicely.

Shown in Figure 3 are the best values of n plotted against log r_e^n for the BCGs. Also shown are the projected $\Delta\chi^2 = 9.21$ ellipses about these points, corresponding to a 99% confidence region (Press et al. 1986). The loose trend (linear correlation coefficient $r = 0.55$, at greater than 99.9% significance) pairs large effective radii, corresponding to large bright galaxies, with large values of n. This change in profile shape with galaxy size can be seen in the template profiles from Figure 1 of Schombert (1987), where the

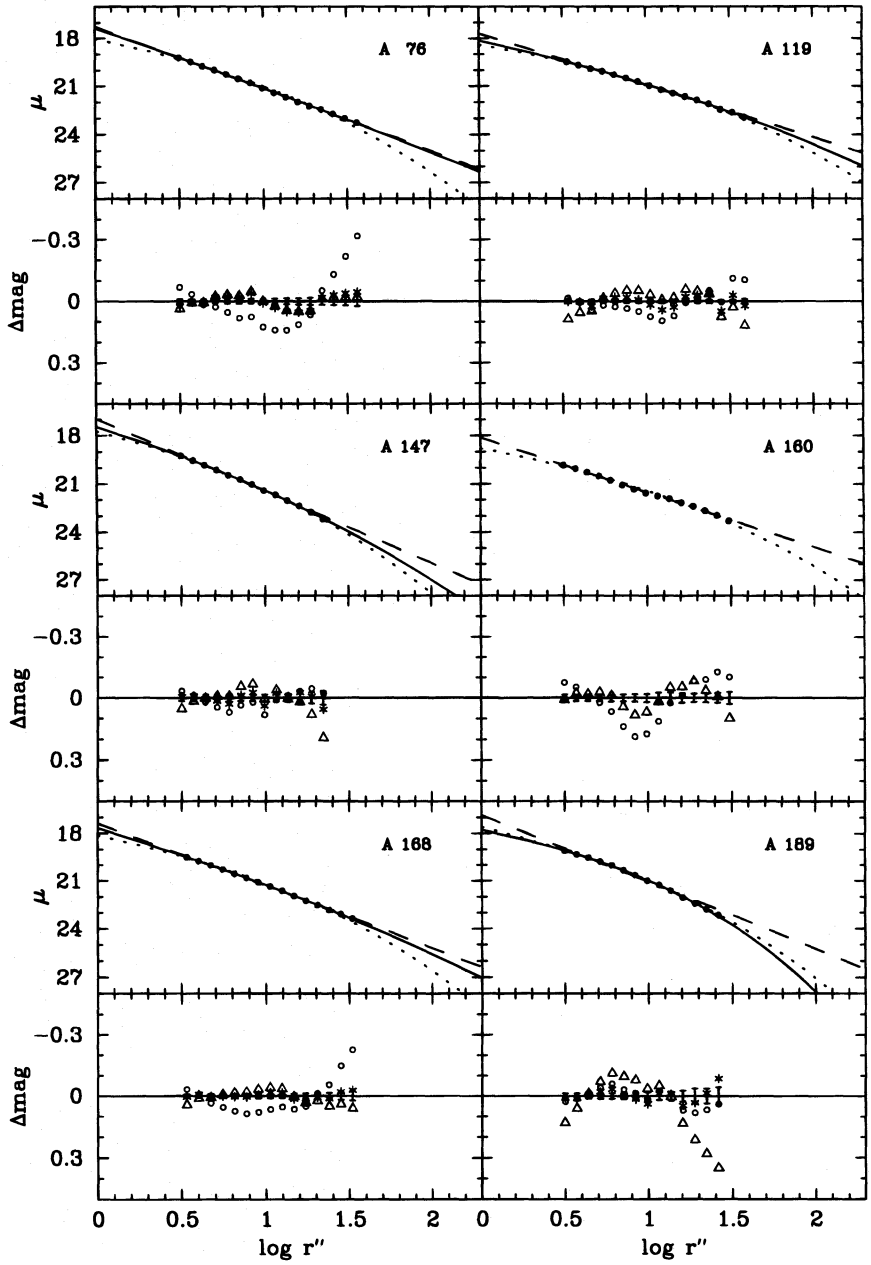

FIG. 2.—We show the surface brightness profiles for a sample of BCGs, together with the best-fitting $R^{1/4}$, (*dotted line*) $R^{1/n}$ (*solid line*) and power law (*dashed line*). The residuals of the profiles about these models are displayed in a magnified portion below the profiles themselves—circles, stars, and triangles for the respective models.

intrinsically bright elliptical galaxies have less curvature than predicted by the $R^{1/4}$ law (high n) and the intrinsically faint elliptical galaxies have too much (low n).

It is pointed out that the profiles have additional wiggles in them that are not accommodated for by the $R^{1/n}$ law and these exist at a level greater than the observational errors. As a result, the reduced χ^2-values for each profile's optimal fit is larger than 1. Given that we have not underestimated our errors, as shown by the good agreement of repeat measurements, this would imply that the model being fitted is inadequate. It is true that there are features/wiggles in the profiles that are not explained by the $R^{1/n}$ law, nor are they explained by the $R^{1/4}$ law. However, the bulk shape of the profile is described better by an $R^{1/n}$ law than an $R^{1/4}$ law, as indicated in Table 1, which shows the reduced χ^2-values for the models fitted to the data. This is illustrated in Figure 4, which has the reduced χ^2-values of each model's optimal fit plotted against the value of n from the $R^{1/n}$ profile fit. One can see some general trends present. As one would expect, the $R^{1/4}$ profile fits are best when the $R^{1/n}$ fits have $n = 4$. The power-law fits are better for larger values of n, which is to be expected, since larger values of n mean a profile with less curvature. The $R^{1/n}$ fits are better than those of the other two models and the quality of the fit appears to be independent of n. As an alternative measure of the errors, we set the reduced $\chi^2 = 1$ for the optimal fit and computed the 1 σ ellipses normalized to this level. These are also shown in Figure 3.

Seeing effects are not responsible for the observed correlation of n with radius. We explored excluding different inner portions of the light profile. Saglia et al. (1993) showed that the effects of seeing on the photometric properties of

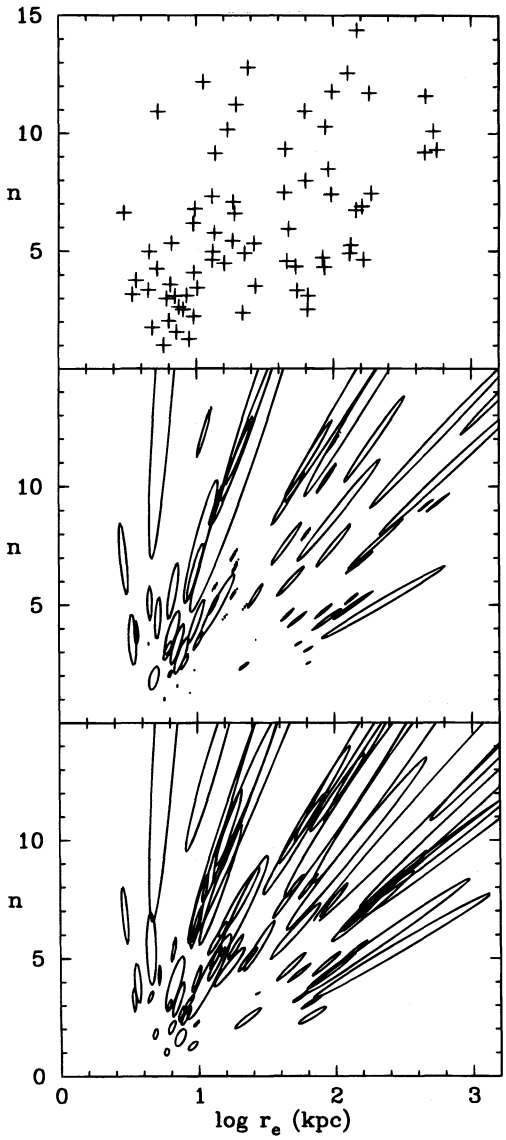

FIG. 3.—(*upper panel*) Plot of n vs. log r_e^n (kpc) for our sample of galaxies (40% of the BCGs had values of $n > 15$); (*middle panel*) 99% confidence regions; (*lower panel*) 1 σ ellipses after the reduced χ^2 has been normalized to 1.

elliptical galaxies can extend as far as 5 seeing disks. Not using the inner 7".5, the same general trend between n and log r_e is still obtained.

Not surprisingly, the $R^{1/n}$ model is the best performer, since it can represent the $R^{1/4}$ profile when $n = 4$ and can approximate a power law for large values of n and fit for profiles of intermediate type. This can be attributed to having one more free parameter than the $R^{1/4}$ or power law. What is important is that such a variety in profiles are real, as indicated by the error ellipses in Figure 3. To explore this further, we simulated a pure $R^{1/4}$ law profile out to $1r_e$ and added to it random Gaussian noise, with standard deviations varying as a function of radius and being derived from the mean S/N errors of the 119 BCGs. We ran a Monte Carlo simulation, solving for r_e^n, μ_0^n, and n each time with a new set of random noise to see if we could explain the range of values in r_e^n and n observed with the real data. Figure 5 shows the entire cloud of solutions, not just the 1 or 2 σ ellipses. Clearly, observational noise cannot explain the claimed trend of n with r_e^n, suggesting that it is physically real and galaxies do indeed exhibit such a range in profile shapes. This analysis does, however, exclude the influence of sky-subtraction errors, which are estimated to be at a level of 0.3%, and should not be significant. In addition, the S/N weighting scheme, employed in the model fitting, will downplay possible contributions from sky-subtraction errors. The possibility, mentioned by Kormendy (1980, 1982), that such a correlation may not be physically significant but rather due to coupling of the parameters in the fitting formula does not fully explain the observed variation in n or the correlation of r_e with n. The error ellipses do indicate a coupling amongst the parameters along the correlation, but they are inadequate to explain the entire correlation. This becomes even more evident in the following section (in particular, Fig. 11), where we consider ordinary elliptical and dwarf galaxies.

In fitting the $R^{1/n}$ formula, it was not possible to obtain meaningful results for all profiles. The flattened profiles had large values of n and implausibly large half-light radii. As the shape parameter increased, it lost its sensitivity and for values of n greater than about 15, the profiles resembled straight lines, asymptoting to r^{-2}. That is, the profiles were better described by a power law. For about 40% of the data it was not appropriate to fit an $R^{1/n}$ law but rather a power law. This can be compared with the work of Ledlow & Owen (1995), who found for a control sample of 50 non–radio-selected galaxies in rich clusters, 39% preferred a power-law fit. The slope and intercept of the best-fitting power law for each BCG is plotted in Figure 6. Not surprisingly, there is a slight trend for galaxies with a steeper profile to have a brighter central flux, represented by the μ intercept at $r = 1''$. Since the power law is appropriate for BCGs with $n > 15$ these galaxies have been marked with a star so as to distinguish them from the other galaxies that are not well represented by a power law. Both types occupy similar regions, with the BCGs well fitted by a power law not occupying any special domain of this diagram. Of course the real galaxy profile must turn over and be truncated at some radius, otherwise it would be of infinite size and luminosity. But for the range in radius explored, some 40% of the BCGs had surface brightness profiles of a power-law nature. Ordinary elliptical galaxies and certainly dE do not show this feature over the same range in radius. It is pointed out that for large values of n, the half-light radius obtained from the $R^{1/n}$ model is not really physical but is, however, an expression of the slope of the galaxy profile measured by the data.

We find no correlation between n and ellipticity. Following Caon et al. (1993), we have plotted n against the maximum ellipticity of the galaxy in Figure 7. We also used the ellipticity at the semimajor axis radius of $10\,h^{-1}$ kpc and again found no evidence for a correlation. Caon et al. (1993) found a range of ellipticities for $n < 4$ but for $n > 4$ the ellipticity was typically less than 0.3. A possible reason for this different result could be that we used BCGs, while Caon et al. (1993) used E/S0 galaxies, indicating a difference between the galaxy classes. Although this seems hard to understand, we note that Caon et al. (1993) only had a dozen galaxies with $n > 4$ and only two with $n > 10$. They also found that this trend disappeared when they used the value of n constructed from the semiminor axis profile.

Figure 8 shows n plotted against the metric magnitude (R), enclosed by a circular aperture of 12.5 kpc (we used a value of $H_0 = 80$ km s^{-1} Mpc^{-1}, and use the CMB refer-

TABLE 1

MODEL PARAMETERS

Ident. Abell	n	log R_e^n [kpc]	μ_e^n [mag]	$R^{1/n}$: log (Reduced χ^2)	log R_e [kpc]	μ_e [mag]	$R^{1/4}$: log (Reduced χ^2)	intercept [mag]	slope	Power-law: log (Reduced χ^2)
76	-	-	-	-	1.15	22.58	2.93	17.26	-1.55	1.95
119	7.4	2.27	26.43	2.17	1.64	23.80	2.66	17.70	-1.29	2.76
147	6.8	0.99	21.99	1.29	0.86	21.38	1.77	16.97	-1.79	1.99
160	-	-	-	-	1.45	23.79	2.59	18.13	-1.36	1.95
168	12.6	2.10	26.69	1.25	1.21	22.66	2.63	17.38	-1.56	2.01
189	3.0	0.78	21.15	1.37	0.85	21.49	1.74	16.85	-1.68	2.69
193	-	-	-	-	1.62	24.01	2.99	18.09	-1.31	2.59
194	-	-	-	-	1.26	22.78	3.83	16.49	-1.36	3.28
195	-	-	-	-	0.88	21.65	2.28	17.21	-1.77	1.37
260	-	-	-	-	1.33	22.84	3.40	17.11	-1.47	1.84
261	-	-	-	-	1.09	22.25	2.88	17.29	-1.66	1.94
262	-	-	-	-	1.35	23.45	3.96	17.05	-1.23	3.18
295	-	-	-	-	1.40	23.37	2.84	17.69	-1.41	1.92
347	-	-	-	-	1.01	22.05	3.88	16.22	-1.57	2.80
376	-	-	-	-	1.46	23.61	2.44	17.98	-1.39	1.36
397	-	-	-	-	1.26	22.84	3.24	17.16	-1.47	2.27
407	4.6	2.22	26.06	2.05	2.04	25.40	2.06	18.92	-1.02	2.32
419	3.6	0.81	21.67	1.88	0.83	21.78	1.89	17.44	-1.76	2.35
496	6.7	2.16	26.00	2.16	1.64	23.85	2.98	17.43	-1.27	3.28
533	4.6	1.12	22.43	1.25	1.06	22.17	1.32	17.44	-1.61	2.15
539	-	-	-	-	1.11	22.40	3.23	16.94	-1.55	1.92
548	-	-	-	-	0.96	21.77	2.49	16.98	-1.70	1.80
569	5.8	1.13	22.53	2.87	0.96	21.71	3.28	16.15	-1.57	3.83
576	6.6	0.47	20.03	1.51	0.51	20.22	2.06	16.64	-2.06	2.34
634	3.1	0.93	21.69	2.70	1.02	22.13	2.93	16.81	-1.54	3.87
671	-	-	-	-	1.47	23.02	3.76	17.27	-1.45	2.62
779	-	-	-	-	1.34	22.38	4.44	16.02	-1.44	2.83
912	3.1	0.84	21.81	1.49	0.89	22.06	1.57	17.62	-1.75	2.20
957	14.5	3.31	30.78	2.35	1.56	23.44	3.28	17.43	-1.35	2.67
999	-	-	-	-	0.88	21.56	3.29	16.64	-1.74	2.09
1016	-	-	-	-	0.76	21.32	3.06	16.83	-1.82	0.72
1060	9.2	2.66	28.32	3.58	1.54	23.83	4.20	16.69	-1.20	4.05
1100	-	-	-	-	1.18	22.53	2.99	17.37	-1.60	1.35
1139	-	-	-	-	1.21	22.84	3.23	17.56	-1.50	1.93
1142	-	-	-	-	1.21	22.78	3.50	17.20	-1.53	2.53
1177	-	-	-	-	1.51	23.59	3.88	17.36	-1.34	2.68
1185	1.3	0.95	21.24	3.50	1.41	23.27	4.08	17.49	-1.29	4.33
1213	3.4	1.01	21.63	2.82	1.06	21.86	2.83	17.12	-1.62	3.11
1228	-	-	-	-	0.85	21.74	3.13	17.10	-1.76	2.06
1257	-	-	-	-	0.65	21.22	2.92	17.21	-1.86	2.57
1267	10.2	1.23	23.42	2.88	0.83	21.54	3.09	16.88	-1.72	2.98
1308	-	-	-	-	1.27	22.71	2.93	17.45	-1.56	1.99
1314	-	-	-	-	1.40	23.16	4.54	17.06	-1.45	3.83
1367	4.5	1.20	22.57	3.38	1.14	22.29	3.40	16.40	-1.45	4.05
1631	8.5	1.96	25.68	2.19	1.35	23.00	2.55	17.53	-1.44	2.50
1644	3.1	1.81	23.90	2.45	2.05	24.79	2.66	18.18	-1.07	3.56
1656	8.0	1.80	24.33	2.38	1.29	22.06	3.74	15.82	-1.47	3.74
1736	11.7	2.26	26.28	2.76	1.35	22.24	3.31	16.62	-1.51	2.98
1836	7.5	1.64	24.34	1.85	1.22	22.47	2.71	17.00	-1.50	2.81
1983	5.3	0.82	21.26	1.04	0.78	21.06	1.52	16.94	-1.86	2.31
2040	-	-	-	-	1.72	24.60	3.37	18.49	-1.21	3.01
2052	3.3	1.73	23.92	2.33	1.90	24.56	2.54	17.91	-1.11	3.68
2063	4.3	1.72	24.45	2.03	1.65	24.17	2.07	17.94	-1.21	3.20
2107	4.6	1.66	23.83	2.46	1.56	23.42	2.52	17.41	-1.32	3.38
2147	5.9	1.67	24.48	2.35	1.38	23.22	2.60	17.37	-1.39	2.98
2151	11.6	2.67	28.65	2.73	1.45	23.50	2.99	17.56	-1.37	2.81
2152	4.2	0.71	20.94	1.08	0.71	20.93	1.11	16.91	-1.94	2.35
2162	-	-	-	-	1.15	22.16	3.13	16.57	-1.59	2.26
2197	10.3	1.94	25.13	3.38	1.25	21.99	3.89	16.13	-1.53	3.66
2199	6.9	2.21	25.93	3.06	1.64	23.62	3.41	17.13	-1.25	3.59
2247	2.0	0.80	21.01	2.20	0.95	21.76	2.68	17.12	-1.64	3.16
2572	-	-	-	-	1.39	23.14	4.08	17.33	-1.48	3.69
2589	-	-	-	-	1.77	24.48	3.08	18.12	-1.20	1.60
2593	2.4	1.34	22.68	2.58	1.69	24.12	2.79	18.02	-1.18	3.26
2634	-	-	-	-	1.48	23.15	3.82	16.93	-1.36	2.60
2657	1.8	0.68	20.88	1.07	0.79	21.46	1.73	17.32	-1.75	2.14
2666	9.3	1.65	24.34	2.41	1.10	21.82	3.15	16.22	-1.56	2.95
2717	-	-	-	-	1.91	25.05	3.23	18.66	-1.13	3.05
2731	6.6	1.28	22.81	3.35	1.07	21.83	3.56	16.38	-1.64	3.75
2806	9.1	1.14	22.75	2.59	0.83	21.28	3.31	16.35	-1.73	3.13
2870	4.9	1.35	23.05	2.80	1.23	22.52	2.99	16.52	-1.45	3.87
2877	-	-	-	-	1.24	21.94	4.54	15.83	-1.50	3.20
2881	-	-	-	-	0.75	21.48	2.28	17.46	-1.88	1.47
2896	-	-	-	-	0.79	21.07	3.01	16.47	-1.81	1.94
2911	-	-	-	-	0.65	21.19	3.35	16.36	-1.80	2.70
3144	-	-	-	-	0.78	21.39	2.33	17.19	-1.88	1.35
3193	5.0	1.12	22.49	1.96	1.04	22.11	2.20	16.96	-1.63	3.09
3367	2.5	0.90	21.68	1.85	1.03	22.27	2.15	17.55	-1.63	2.76
3374	1.0	0.76	20.67	2.43	0.93	21.55	3.20	17.14	-1.72	3.41
3376	-	-	-	-	1.20	22.25	2.92	17.01	-1.60	2.03

TABLE 1—*Continued*

Ident. Abell	n	log R_e^n [kpc]	μ_e^n [mag]	$R^{1/n}$: log (Reduced χ^2)	log R_e [kpc]	μ_e [mag]	$R^{1/4}$: log (Reduced χ^2)	intercept [mag]	slope	Power-law: log (Reduced χ^2)
3381	14.4	2.17	27.66	1.54	1.09	22.79	2.38	17.69	-1.57	1.81
3389	2.2	0.98	21.29	2.81	1.24	22.45	3.64	16.77	-1.39	4.27
3395	4.3	1.93	24.73	2.28	1.86	24.45	2.29	18.09	-1.17	2.97
3526	3.5	1.43	22.69	2.91	1.53	23.10	3.36	15.79	-1.21	5.02
3528	-	-	-	-	1.68	23.78	3.35	17.69	-1.33	2.33
3530	11.5	3.78	31.47	2.86	1.97	24.50	3.05	18.02	-1.14	2.92
3532	-	-	-	-	1.89	24.66	3.19	18.27	-1.22	2.22
3537	7.1	1.27	22.78	3.22	0.97	21.40	3.66	15.46	-1.58	3.80
3542	10.9	0.72	21.38	1.78	0.64	20.94	2.16	16.85	-1.94	1.95
3553	2.6	0.87	21.95	1.00	0.96	22.36	1.38	17.88	-1.72	2.10
3554	4.9	2.12	25.55	2.84	1.90	24.70	2.86	18.33	-1.12	3.11
3556	5.3	1.42	22.94	2.35	1.28	22.31	2.51	16.90	-1.55	3.05
3558	5.2	2.13	25.08	2.30	1.87	24.04	2.69	17.51	-1.22	3.49
3559	-	-	-	-	1.58	23.47	3.31	17.48	-1.34	2.91
3560	3.3	0.65	20.65	2.88	0.69	20.88	3.08	15.40	-1.67	4.20
3562	-	-	-	-	1.84	24.39	3.72	17.90	-1.26	2.71
3564	4.1	0.98	22.01	1.26	0.98	21.99	1.26	17.42	-1.73	2.31
3565	11.8	1.99	25.90	3.01	1.08	21.81	4.34	15.34	-1.51	3.81
3566	-	- -	-	-	0.65	20.73	2.32	16.97	-2.03	1.61
3570	3.8	0.56	20.21	2.01	0.56	20.20	2.02	16.40	-2.04	2.73
3571	2.5	1.81	23.30	3.33	2.21	24.84	3.55	17.74	-1.03	4.09
3572	5.0	0.66	20.57	2.27	0.66	20.57	2.32	16.48	-2.00	2.79
3574	9.3	2.75	28.13	3.79	1.61	23.56	4.13	16.52	-1.20	4.02
3575	3.2	0.53	20.96	1.02	0.53	20.95	1.17	17.33	-2.02	2.01
3581	-	-	-	-	1.25	22.96	3.34	16.84	-1.43	2.42
3656	-	-	-	-	1.17	22.12	4.34	15.97	-1.47	2.57
3676	1.6	0.86	20.88	3.24	1.06	21.91	3.58	16.92	-1.60	3.85
3677	7.3	1.11	22.95	1.18	0.92	22.01	1.55	17.56	-1.74	1.64
3698	11.2	1.29	23.47	2.56	0.79	21.10	3.41	15.88	-1.69	3.00
3716	10.1	2.73	28.51	2.19	1.62	23.94	2.64	17.87	-1.30	2.44
3733	-	-	-	-	1.30	23.20	3.35	17.58	-1.46	2.46
3736	7.4	1.98	25.05	1.67	1.51	23.00	2.68	17.06	-1.44	2.81
3742	12.2	1.05	22.74	2.86	0.65	20.77	3.76	15.56	-1.78	3.28
3744	12.8	1.38	23.82	2.13	0.88	21.46	2.68	16.76	-1.75	2.31
3747	5.4	1.26	22.88	2.44	1.11	22.18	2.86	16.74	-1.54	3.57
3869	6.2	0.98	22.04	1.51	0.88	21.53	2.03	16.93	-1.78	2.45
4038	10.9	1.79	25.50	2.19	1.08	22.26	3.17	16.78	-1.57	2.77
4049	-	-	-	-	1.13	22.41	4.16	16.72	-1.58	3.25
4059	4.7	1.92	24.52	2.25	1.78	23.93	2.37	17.63	-1.24	3.29

NOTE.—Reduced χ^2 value of the best fitting $R^{1/n}$, $R^{1/4}$, and power-law model is shown for each BCG, along with the parameters from the fit. R_e and R_e^n are the effective half-light radii of the $R^{1/4}$ law and the $R^{1/n}$ law, respectively, with μ_e and μ_e^n the surface brightness at these points. For values of $n > 15$, the $R^{1/n}$ fitting function fails to produce meaningful results.

ence frame here). A linear correlation coefficient of -0.17, at a significance level of 84%, suggests that there is little correlation between these two values for our BCG sample. This is not surprising given the small scatter in metric magnitudes for the BCGs—only 0.33 magnitudes. That the BCG metric magnitude is not significantly influenced by the galaxy profile shape, represented by n, eliminates the chances of another hidden variable giving scatter to this magnitude, which has been used as a distance indicator by Lauer & Postman (1994) and Colless (1995) in their studies of peculiar velocity flows.

5. $R^{1/n}$ UNIVERSALITY

What influences the profile shape of galaxies? Is it caused by environment, changes arising due to dynamical evolution, differing formation history, or individual galaxy peculiarities such as dust clouds or rings, lenses, shells, ripples, etc.? The trend of n with galaxy size argues against such peculiarities being responsible, as this would require these features to be correlated with galaxy size. There is also no indication in these BCGs of an embedded disk. However, the small wiggles in the profiles that are not accommodated by the $R^{1/n}$ law are at a significance level greater than accounted for by the observational uncertainty and may be a sign of such peculiarities (Lauer 1988). A close analysis of the two-dimensional residual maps (images with the best-fitting $R^{1/n}$ law subtracted) could reveal such features.

To investigate possible environmental effects on the BCG profile shape, we checked for a correlation between n and richness class, RC, (Abell 1958) and n and Bautz-Morgan type, BM, (Bautz & Morgan 1970). We only used those galaxies that had values of $n < 15$, being some 60% of our sample. No obvious trend was found for either case, as can be seen in Figures 9 and 10, respectively. We point out that the profile shape has been determined from the inner surface photometry (<23.5 mag) and is thus free from outer galaxy distortions such as envelopes, which may be influenced by the environment. Einasto & Caon (1996) have shown n not to correlate with galaxian density for their sample of E/S0 galaxies, thereby further restricting the possibility of environment being responsible for the shape parameter n.

BCGs typically like values of n greater than 4. This is not only interesting in itself, but becomes more so when we note that studies of dE galaxies show them to have values of n typically less than 4. Caon et al. (1993) show that ordinary elliptical and S0 galaxies show a range in n above and below 4. Continuing Figure 5 of Caon et al. (1993) we add our data to produce Figure 11, showing the continued relationship between galaxy structure and size for dwarf galaxies, ordinary E/S0 galaxies, and BCGs. It becomes apparent that n

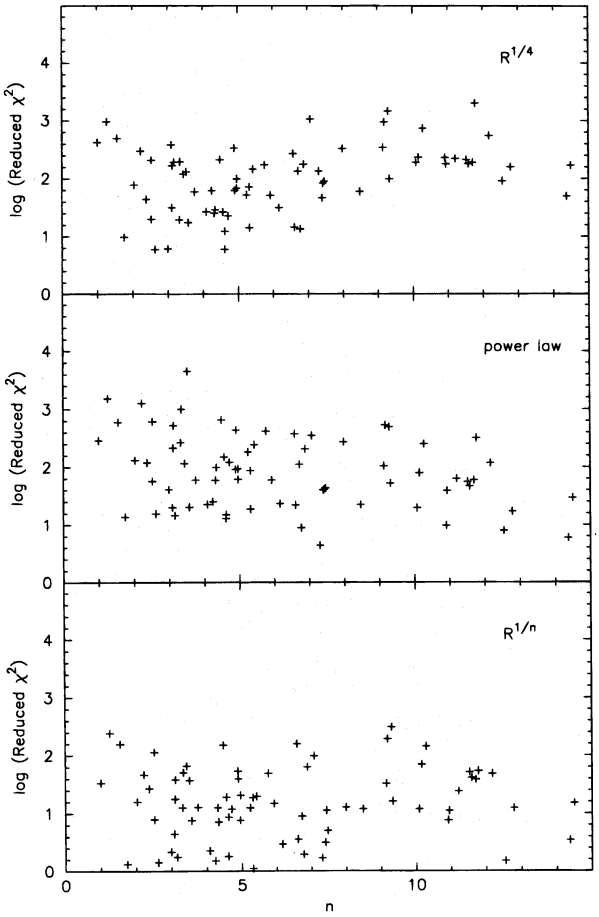

FIG. 4.—Reduced χ^2-values from the optimal fit of the $R^{1/4}$, power law, and $R^{1/n}$ models to the BCG profiles are shown here against the value of n from the optimal $R^{1/n}$ fit.

is not just some randomly scattered extra parameter whose only purpose is to reduce the χ^2 ellipses of our models, but is a significant physical attribute that describes the galaxy light profile shape. Caon et al. (1993) fitted the $R^{1/n}$ law to the B-band photometry of 33 E/S0 galaxies. While we used the Kron-Cousins R band to image our sample of BCGs, changes in profile shape due to color gradients are expected to be lost in the scatter of Figure 11. We note that the values of r_e from Caon et al. (1993) are not those from their model but are derived directly from the galaxy light profile. The dwarf galaxies are a sample of 187 Fornax cluster

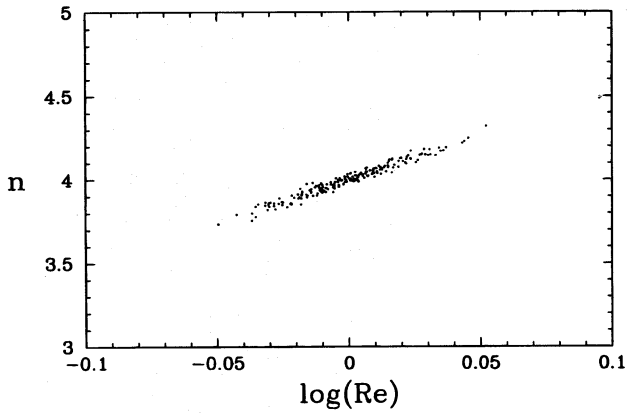

FIG. 5.—Cloud of solutions from a Monte Carlo investigation of the contribution to the $n - \log r_e^n$ relation from observational errors.

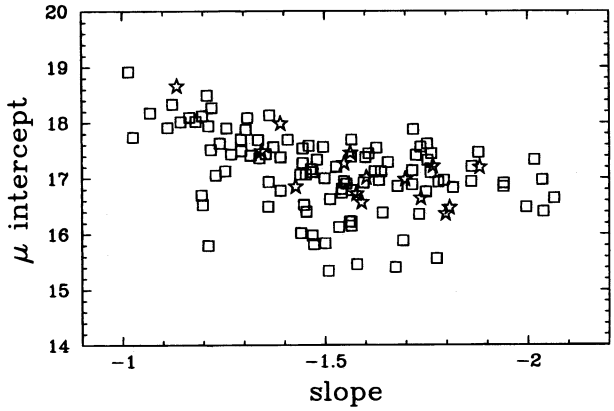

FIG. 6.—Plot of the best-fitting power-law slope and intercept at $r = 1''$ for the BCGs. Those galaxies fitted with a value of $n > 15$ from the $R^{1/n}$ model are marked with stars, those fitted with a value of $n < 15$ are marked with squares. The 1 σ error bars are smaller than the graph markers.

dwarfs from Davies et al. (1988). They fitted a variant form of the $R^{1/n}$ law to the B-band images, such that $I(r) = I_0 \exp[-(r/A)^N]$. By setting $N = 1/n$, one has $r_e'' = A''(2/N - 0.327)^{1/N}$. We used a value of $H_0 = 80$ km s^{-1} Mpc^{-1} throughout in determining the value of r_e kpc.

Thus, we have a parameter that traces structural differences amongst galaxies having a large range in size. The fact that the $R^{1/n}$ profile is applicable over such a range (6 orders of magnitude in the mass) suggests that there are similar formation mechanisms present for all these galaxies. Violent

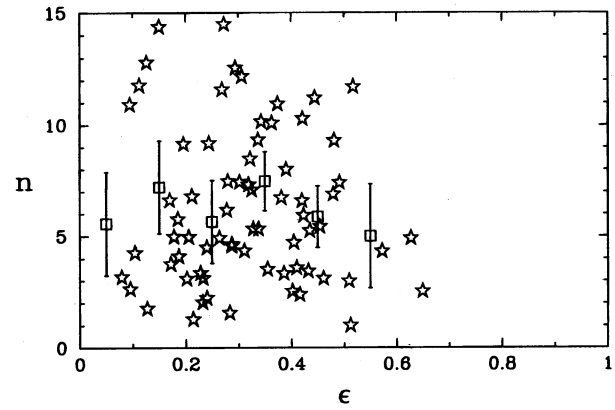

FIG. 7.—Plot of n vs. the maximum ellipticity of the BCGs. Also shown is the mean and sample standard deviation in bins of 0.1 in ellipticity.

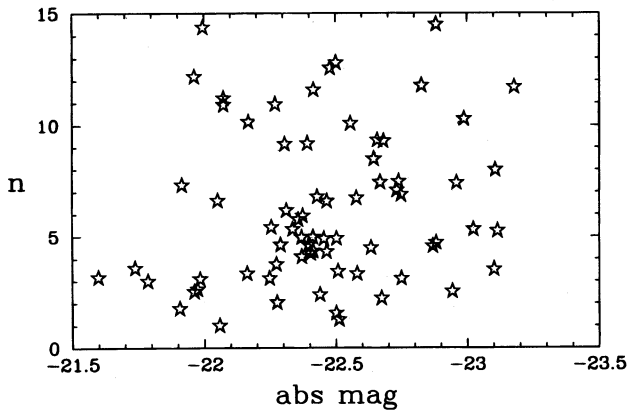

FIG. 8.—Plot of n vs. the metric magnitude contained with $10\,h^{-1}$ kpc

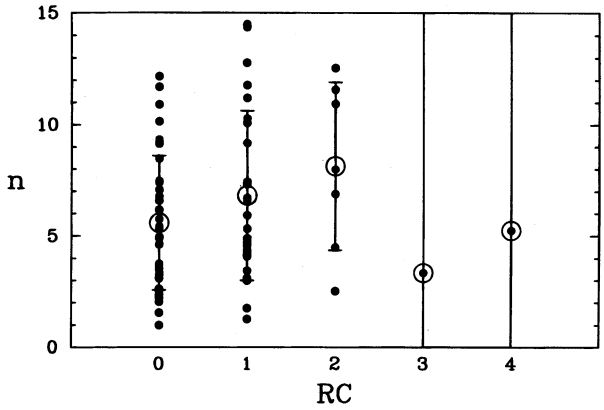

FIG. 9.—Galaxy shape parameter, n, is plotted vs. the galaxy cluster richness class, RC. Also shown are the mean values for each class and the associated standard deviation.

relaxation (Lynden-Bell 1967) followed by a redistribution of weakly bound stars to larger radii and an escape of stars with positive energies results in a stellar phase space having a distribution function $f(E)$ that is well described by a Maxwell-Boltzmann distribution for the central parts of the galaxy (Hjorth & Madsen 1991). Theoretical modeling of the physics of violent relaxation has shown that the shape parameter n is dependent on the dimensionless central

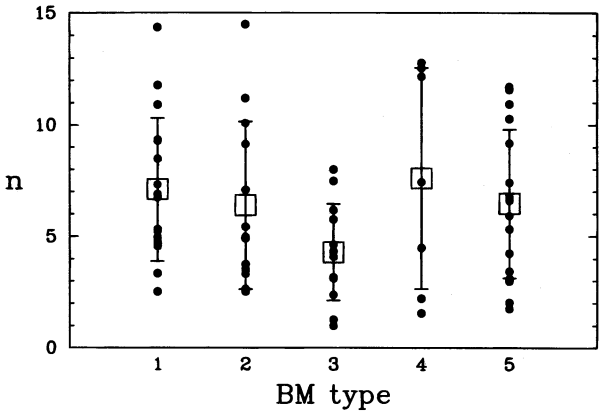

FIG. 10.—Galaxy shape parameter, n, is plotted vs. the Bautz-Morgan, BM, type for the galaxy cluster. Also shown are the mean values for each BM type and the associated standard deviation.

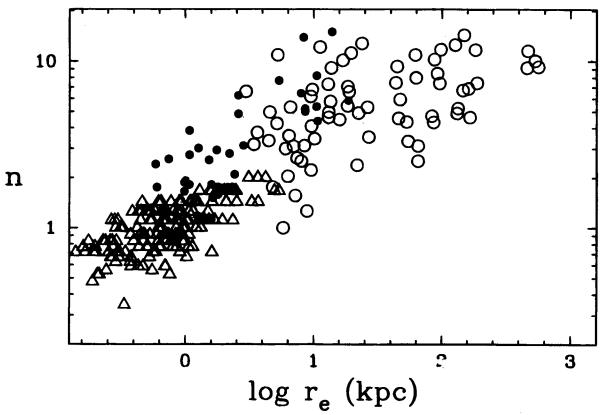

FIG. 11.—Galaxy shape parameter, n, is plotted vs. the logarithm of the effective half-light radius, r_e kpc, for a sample of dwarf galaxies (Davies et al. 1988) (*triangles*), ordinary E/S0 galaxies (Caon et al. 1993) (*filled circles*), and our BCG data (*open circles*).

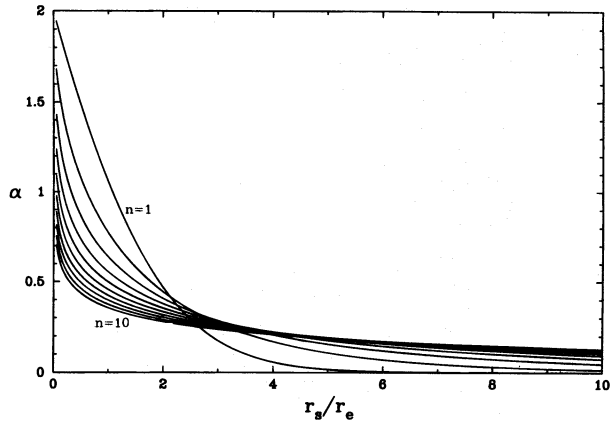

FIG. 12.—Structure parameter, α, is plotted as a function of radius for different values of the shape parameter, n, from the $R^{1/n}$ model. r_s/r_e is the ratio of the sampling radius, at which α is computed, to the effective half-light radius of each respective model.

potential, either normalized to the central velocity dispersion (like in the King model) or a global measure of the potential (Hjorth & Madsen 1995). Galaxies with larger central potentials result in galaxies with larger values of n, and those with smaller potentials have values of n less than 4. Conversely, Ciotti (1991) has shown that for an $R^{1/n}$ law, the central potential increases as n does. This suggests that the bulk shape of an elliptical galaxy's luminosity profile is not due to its individual genetic peculiarities (i.e., dust lanes, shells, etc.), or its environment, but rather something intrinsic to each galaxy, being the mass distribution. It has previously been suggested by Young & Currie (1994) that n may be a function of the galaxy's gravitational potential well and hence its mass. Andredakis et al. (1995) have also proposed that n may be dependent on the galaxy's intrinsic properties such as its total mass or size. We hope to investigate this further when we have velocity dispersion data for the BCGs. This information can be used to estimate the mass of each galaxy (Michard 1980; van Albada, Bertin, & Stiavelli 1995), which we can then check for a correlation with n.

6. LOCAL PROFILE STRUCTURE α

The shape parameter, n, describes the overall global shape of the galaxy light profile (with the exception of extended envelopes in cD galaxies). There is another measure of a galaxy's light profile curvature, referred to as

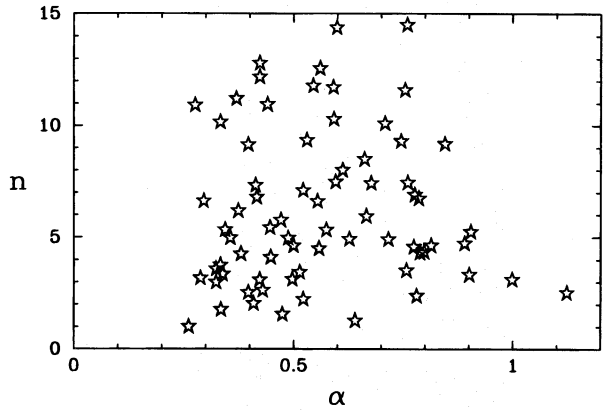

FIG. 13.—Plot of n vs. α, where α is taken from Lauer & Postman (1994).

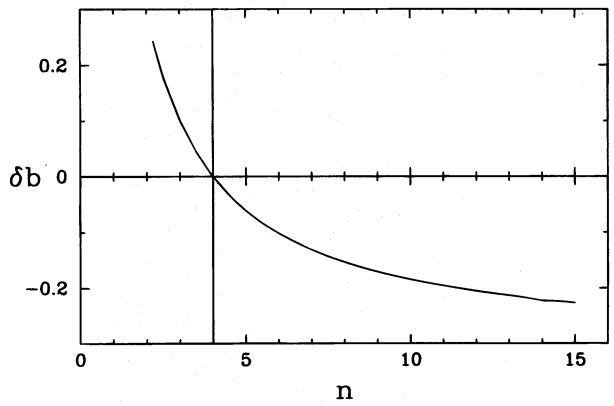

FIG. 14.—Series of $R^{1/n}$ profiles were constructed, from which we computed δb (Burkert 1993). The relation between these two measures of the galaxy light profile curvature are shown.

the structure parameter by Hoessel (1980) and given by $\alpha = d \ln L/d \ln r|_{r_s}$. It is a measure of the galaxy profile at a given sampling radius, r_s. Lauer & Postman (1994) and Colless (1995) have used α because of its correlation with metric magnitude and hence ability to create improved standard candles for distance measurements. In each case, α was measured directly from the light profiles at a sampling radius of 10 h^{-1} kpc. It is, however, possible for one to compute α from the fitted model profile (Graham 1996). Whether this is preferred or not, one gains insight into how α varies for different values of n. Working from equation (3) and assuming zero ellipticity for simplicity, it can be shown that

$$\alpha = \frac{e^{-x}x^{2n}}{n\gamma(2n, x)} . \quad (6)$$

A set of $R^{1/n}$ profiles were constructed and α computed as a function of radius for each, the results of which are shown in Figure 12. For a fixed sampling radius, r_s, α is seen to increase as the effective half-light radius increases. Working against this is the fact that as galaxies get bigger, i.e., larger r_e, they tend to be described by a profile with a larger value of n, as seen in Figure 3. Now profiles with a larger values of n are seen to have smaller values of α for the same ratio of sampling radius to effective half-light radius. The degree to which α changes for a given change in sampling radius or change of n is dependent on the part of the profile one is looking at.

We have plotted the values of n against α for our sample of BCGs that have values of $n < 15$ in Figure 13. Values of α have been taken from Lauer & Postman (1994) rather than computed from the fitted profile model. It seems likely that the reason no trend is evident between these two parameters is because of the competing situation described above.

7. ANOTHER SHAPE PARAMETER

An alternative approach to quantifying the systematic deviations from an $R^{1/4}$ law was taken by Burkert (1993). The observational data in the range $0.6 < x < 1.1$ were fitted by the form $\mu(x) = \mu_0 + bx$, where $x = (r/X_e)^{1/4}$ and X_e is the effective half-light radius of the model. In general, μ_0 and b are dependent on the fitted range in x, which is in turn dependent on the value of X_e. As we do not have a prior knowledge of the value of X_e, this dependence means that our expression must be solved via an iterative process until convergence, such that $X_e^{\rm new} = X_e^{\rm old}(8.3268/b)^4$, with b the best-fitting slope using $X_e^{\rm old}$.

Burkert observed that many galaxy profiles had a characteristic dip/hump about the best-fitting $R^{1/4}$ law. When the dip ($\mu_{\rm galaxy} - R^{1/4}$) was a minimum, it was found to turn over near $x = 0.8$, and when it was a maximum it would be near $x = 0.9$. See Burkert (1993) for a fuller description and profiles. The above mentioned range in x was then cut into two parts, with the division at $x_{\rm cut} = 0.8$ if the dip was a minimum or at $x_{\rm cut} = 0.9$ if it was a maximum. The quantity

$$\delta b = \left(\frac{\partial u}{\partial x}\bigg|_{x \in [x_{\rm cut}; 1.1]} - \frac{\partial u}{\partial x}\bigg|_{x \in [0.6; x_{\rm cut}]} \right) \Big/ 8.3268 \quad (7)$$

was shown to correlate with both absolute magnitude and the mean deviation of the galaxy data about the best-fitting $R^{1/4}$ law. Burkert showed that the brighter galaxies had the more negative values of δb and the fainter galaxies had the more positive values.

This parameter reflects the curvature present in the galaxy profiles that the $R^{1/4}$ law cannot accommodate. However, its extraction is somewhat fiddly and requires the fitting function be applied several times, whereas the $R^{1/n}$ profile is fitted once. A series of $R^{1/n}$ profiles were created, and the method of Burkert was applied to obtain the parameter δb for each. The relation between n and δb is shown in Figure 14. The sense and amplitude of n and δb are in agreement, such that the bigger brighter galaxies with $n > 4$ relate to $\delta b < 0$ and the galaxies with $n < 4$ have $\delta b > 0$.

8. CONCLUSIONS

The nature of the $R^{1/n}$ law is such that as n increases, the galaxy surface brightness profile flattens, and asymptotes toward a power law of slope -2. BCGs typically have values of n greater than 4—i.e., their light profiles are less curved than the classic $R^{1/4}$ law; 40% of our sample is well described by a power law. The range in profile shapes is real and not due to noise in the galaxy profiles or due to a coupling of the three parameters in the model. There is a trend between n and the half-light radius such that the larger galaxies have larger values of n. This trend appears to be a continuation of that noticed for dE galaxies through normal E and S0 galaxies and on to BCGs, suggesting some common physical processes might be at play in the formation of all of these galaxies. This global shape parameter, n, is shown to be independent of richness class and Bautz-Morgan type, suggesting that the galaxy environment (insofar as RC and BM type represent this) is not responsible for the shaping of the bulk distribution of stars in the galaxy. We note that our analysis excludes the outer envelopes of the cD galaxies.

While n is a global measure of the galaxy's light profile (with the exclusion of possible cD envelopes), α is a measure the galaxy's structure at a point. α is shown to be related to n and r_e in an opposing manner. As one moves to larger galaxies, n increases causing α to decrease but at the same time r_e increases causing α to increase. The dominating factor depends on which part of the profile one samples the value of α.

We wish to thank Roberto Saglia and the referee, James Schombert, for their useful comments and suggestions on this paper. We are indebted to Jens Hjorth for his reading of and input to this work. Joe Morris is also thanked for help given during the preparation of this study.

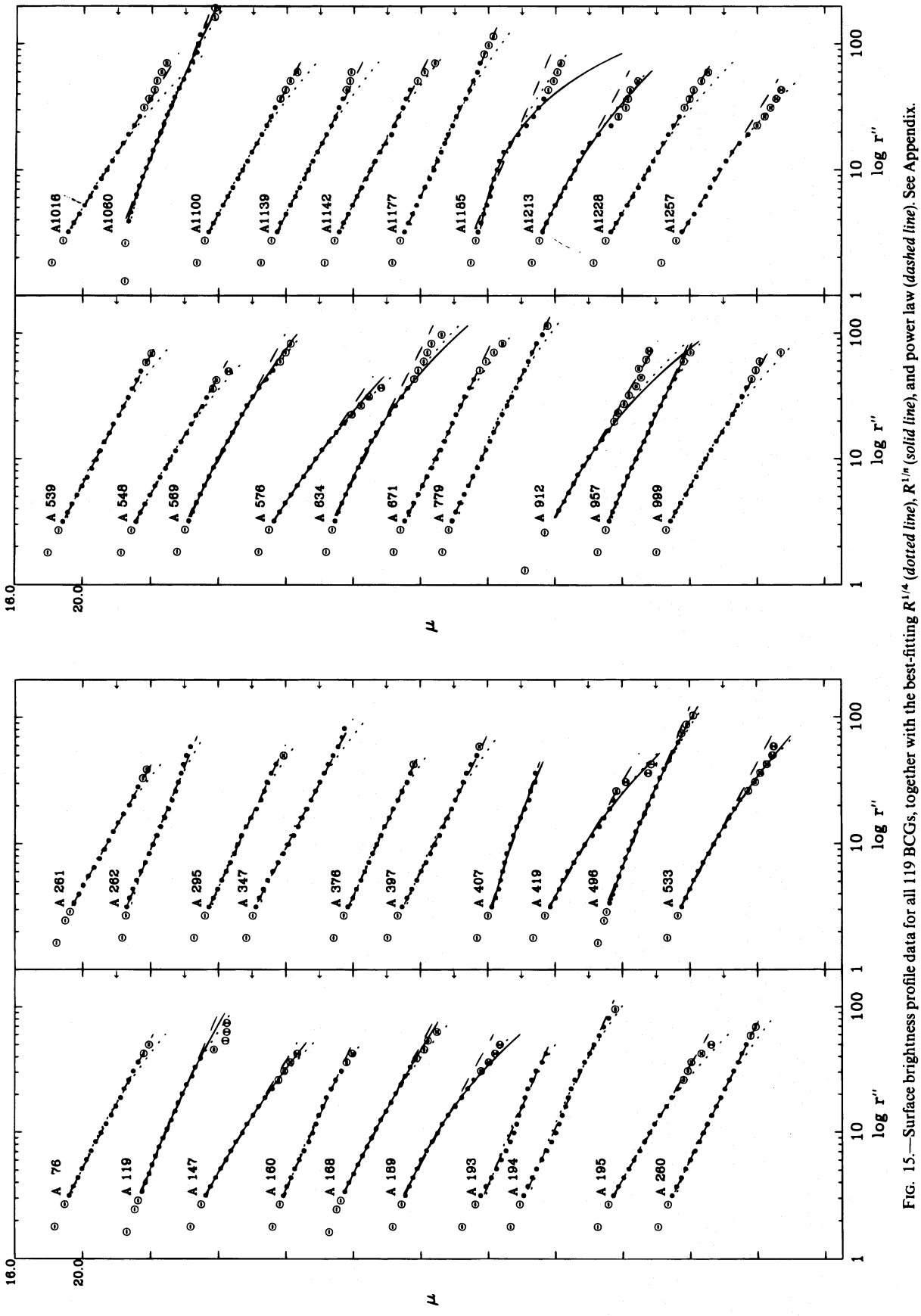

FIG. 15.—Surface brightness profile data for all 119 BCGs, together with the best-fitting $R^{1/4}$ (*dotted line*), $R^{1/n}$ (*solid line*), and power law (*dashed line*). See Appendix.

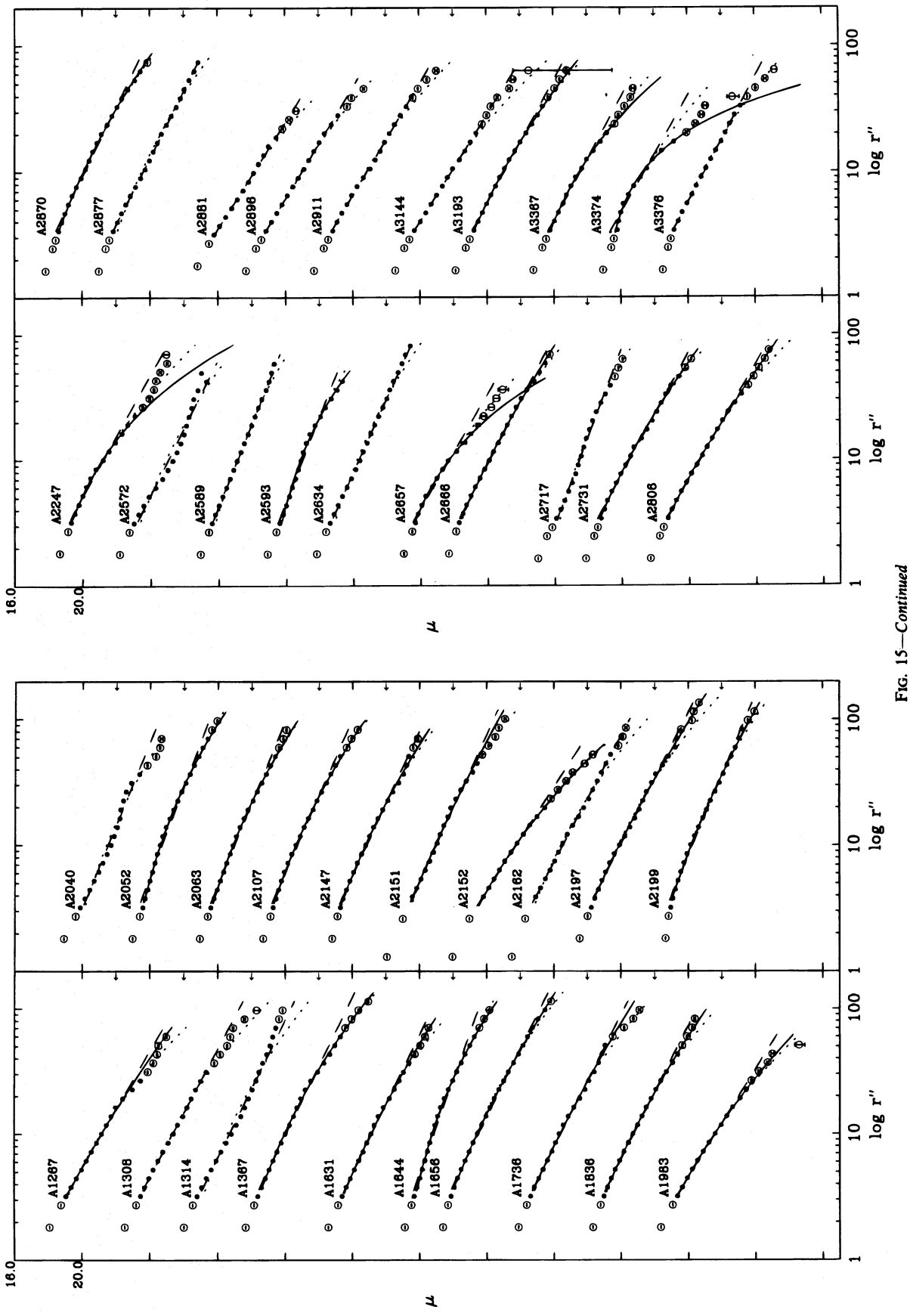

FIG. 15—*Continued*

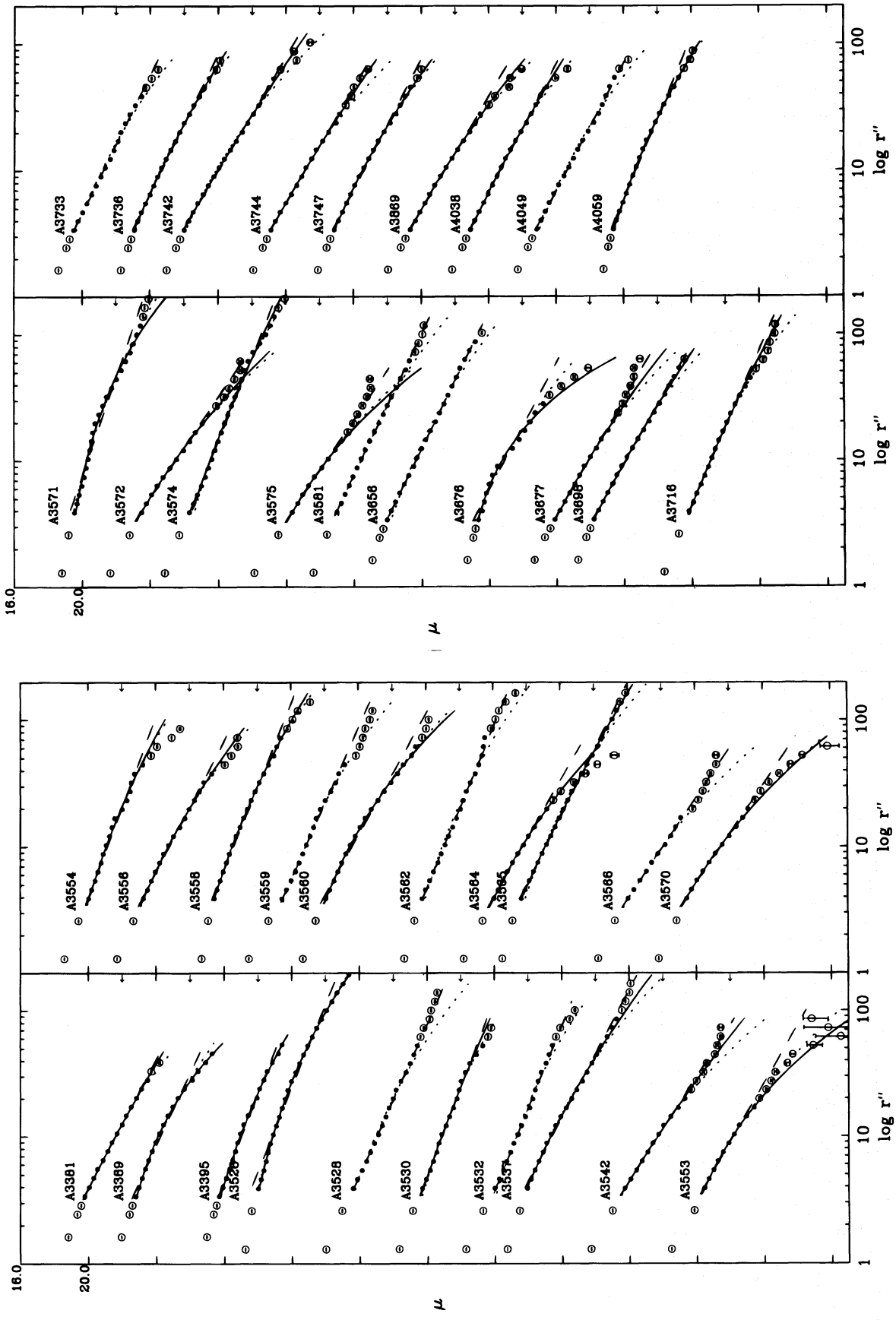

FIG. 15—*Continued*

APPENDIX

BRIGHTEST CLUSTER GALAXY SURFACE BRIGHTNESS PROFILES

The surface brightness profile data for all 119 BCGs, together with the best-fitting $R^{1/4}$ (*dotted line*), $R^{1/n}$ (*solid line*), and power law (*dashed line*) are displayed in Figure 15. The models were fitted to the error-weighted data brighter than 23.5 mag (Kron-Cousins R band) and outside 3″ (*filled circles*). Data outside this range are depicted by an open circle. The S/N errors are shown but usually are contained within the data point symbol. The surface brightness level at 22.0 mag is indicated for each profile by a small arrow on the right hand margin. No $R^{1/n}$ profile is shown when $n > 15$.

REFERENCES

Abell, G. O. 1958, ApJS, 3, 211
Andredakis, Y. C., Peletier, R. F., & Balcells, M. 1995, MNRAS, 275, 874
Bautz, L. P., & Morgan, W. W. 1970, ApJ, 162, L149
Burkert, A. 1993, A&A, 278, 23
Caon, N., Capaccioli, M., & D'Onofrio, M. 1993, MNRAS, 265, 1013
Capaccioli, M. 1989, in The World of Galaxies, ed. H. G. Corwin, & L. Bottinelli (Berlin: Springer), 208
Capaccioli, M., Caon, N., & D'Onofrio M. 1993, MNRAS, 259, 323
Ciotti, L. 1991, A&A, 249, 99
Colless, M. 1995, AJ, 109, 1937
Courteau, S., de Jong, R. S., & Broeils, A. H. 1996, ApJ, 457, 1
Davies, J. I., Phillips, S., Cawson, M. G. M., Disney, M. J., & Kibblewhite, E. J. 1988, MNRAS, 232, 239
de Vaucouleurs, G. 1948, Ann d'Astrophys., 11, 247
———. 1953, MNRAS, 113, 134
de Zeeuw, T., & Franx, M. 1991, ARA&A, 29, 239
Einasto, M., & Caon, N. 1996, MNRAS, submitted
Graham, A.-W. 1996, ApJ, 459, 27
Gunn, J. E., & Oke, J. B. 1975, ApJ, 195, 255
Hausman, M. A., & Ostriker, J. P. 1978, ApJ, 224, 320
Hjorth, J., & Madsen, J. 1991, MNRAS, 253, 703
———. 1995, ApJ, 445, 55
Hoessel, J. G. 1980, ApJ, 241, 493
Hoessel, J. G., Oegerle, W. R., & Schneider, D. P. 1987, AJ, 94, 1111
Humason, M. L., Mayall, N. V., & Sandage, A. R. 1956, AJ, 61, 97
Kormendy, J. 1980, in ESO Workshop on Two-Dimensional Photometry, ed. P. Crane & K. Kjär (Garching: ESO), 191
———. 1982, in Morphology and Dynamics of Galaxies, ed. L. Martinet & M. Mayor (Sauverny: Geneva Obs.), 113
Kormendy, J., & Djorgovski, S. 1989, ARA&A, 27, 235
Lauer, T. R. 1986, ApJ, 311, 34
———. 1988, ApJ, 325, 49
Lauer, T. R., & Postman, M. 1992, ApJ, 400, L47
———. 1994, ApJ, 425, 418
Ledlow, M. J., & Owen, F. N. 1995, AJ, 110, 1959
Lynden-Bell, D. 1967, MNRAS, 136, 101
Michard, R. 1980, A&A, 91, 122
Oegerle, W. R., & Hoessel, J. G. 1991, ApJ, 375, 15
Oemler, A. 1976, ApJ, 209, 693
Ostriker, J. P., & Tremaine, S. D. 1975, ApJ, 202, L113
Postman, M., & Lauer, T. R. 1995, ApJ, 440, 28
Press, W. H., Flannery, B. P., Teukolsky, S. A., & Vetterling, W. T. 1986, Numerical Recipes (Cambridge: Cambridge Univ. Press)
Sandage, A. 1972a, ApJ, 173, 485
———. 1972b, ApJ, 178, 1
Saglia, R. P., Bertschinger, E., Baggley, G., Burstein, D., Colless, M., Davies, R. L., McMahan, R. K., & Wegner, G. 1993, MNRAS, 264, 961
Schechter, P. 1976, ApJ, 203, 297
Schneider, D. P., Gunn, J. E., & Hoessel, J. G. 1983, ApJ, 268, 476
Schombert, J. M. 1986, ApJS, 60, 603
———. 1987, ApJS, 64, 643
Sersic, J.-L. 1968, Atlas de Galaxias Australes (Cordoba: Obs. Astronomico)
Tremaine, S. D., & Richstone, D. O. 1977, ApJ, 212, 311
van Albada, T. S., Bertin, G., & Stiavelli, M. 1995, MNRAS, 276, 1255
Young, C. K., & Currie, M. J. 1994, MNRAS, 268, L11